DETECTION AND LOCALIZATION OF TRAILING EDGE DISBOND IN A LARGE WIND TURBINE BLADE

S. Hoell & P. Omenzetter, *The LRF Centre for Safety and Reliability Engineering, The University of Aberdeen, UK*

ABSTRACT

Efficient wind energy harvesting becomes more and more important as a consequence of the increasing interest in renewable energy in the European Union [1]. This leads to growing sizes of wind turbines (WTs), and with it, larger WT blades (WTBs). The structural designs of these WTBs are created to optimize the potential energy output, where low mass is a key requirement. However, high flexibilities and lower buckling capacities are further results of these developments [2], thus certain damage scenarios become significant. Intelligently designed structural health monitoring (SHM) systems can help to reduce the associated operations and maintenance costs. Even though, several techniques are already developed for structural damage detection (SDD) in WTBs, the majority of these methods is not suitable for in-service measurements. This paper presents a SDD and structural damage localization (SDL) method based on the partial autocorrelation function (PACF) of vibration responses. The approach is applied to a numerical model of a large WTB, where the acceleration responses are obtained from transient dynamic simulations with a simplified aerodynamic loading approach. The novel damage sensitive feature (DSF) is developed as the Mahalanobis distance between a baseline and current vector of PACF coefficients. First, numerical modal analysis of the finite element (FE) WTB model is performed in order to estimate the effect of a disbonding damage scenario on the vibration characteristics. Second, the behaviour of the PACF for time series of the healthy system is discussed. Third, the SDD results on the basis of statistical hypothesis testing are assessed for two selected sensor locations and increasing damage extents. Finally, the performance of the proposed DSF with respect to SDL is illustrated for multiple locations on the WTB's surface. This study demonstrated the efficiency of a DSF based on the PACF for SDD and SDL, which is promising for future developments of vibration-based SHM techniques in WTBs.

NOMENCLATURE

ACF	Autocorrelation Function
AR	Autoregressive
DOF	Degree of Freedom
DSF	Damage Sensitive Feature
FE	Finite Element
NREL	National Renewable Energy Laboratory
PACF	Partial Autocorrelation Function
SDD	Structural Damage Detection
SDL	Structural Damage Localization
SHM	Structural Health Monitoring
SNL	Sandia National Laboratory
WT	Wind Turbine
WTB	Wind Turbine Blade

1. INTRODUCTION

The interest of the European Union in renewable energy [1] leads to developments of offshore wind farms with large-scale WTs. However, the growing sizes and remote erections of WTs lead to increasing operation and maintenance expenditures, which can make up to 20% of the total energy production costs [3]. Additionally, inspections and unforeseen operational problems cause downtimes where no energy can be produced. Thus, the expected revenue and reliability of offshore wind energy production may be reduced. The use of intelligently designed SHM systems can help to counteract this. These systems can reduce inspection efforts, enable to schedule maintenance operations depending on the

structural state and can prevent catastrophic failures.

Although, SDD in WTBs deserves high attention due to significant failure rates compared to other structural components [4], the majority of existing methods are not suitable for in-situ investigations, e.g. ultrasonic, thermal imaging and X-radioscopy methods. Only acoustic emission and strain monitoring methods are currently available for on-site SHM systems in WTBs [5]. However, these methods require dense arrays of sensors, because only local damages can be detected. Thus, high instrumentation and data analysis costs are consequences.

Vibration-based techniques are generally less demanding with respect to instrumentation efforts because they utilize changes in global vibration responses. Methods that use modal parameters, such as natural frequencies, modal damping ratios and mode shapes, for SDD are mature [6]. However, they require the estimation of these parameters, and for large structures, this can only be done using output-only data. The operational modal analysis methods developed for that purpose are computationally demanding and difficult to automatize [7].

Time series methods, as data-driven approaches, are favourable because they enable to avoid this estimation step. These methods can be divided into two groups. The first group utilizes differences between coefficients of estimated parametric models of response signals. The theoretical relationship between structural stiffness and autoregressive (AR) coefficients was demonstrated by Nair et al. [8], and multivariate AR models were used for condition monitoring of a 5 MW offshore WT [9].

However, the use of parametric models requires a priori selection, identification and validation of such models. This can be avoided by non-parametric time series representations, which are the second group of time series SDD methods. Autocorrelation functions (ACFs) were used for SDD in a WTB by Hoell and Omenzetter [10]. Even though, damage of moderate size was detected, the detectability of early damage was noticeably affected when sensor noise was added.

The approach proposed in this paper uses PACFs obtained from acceleration responses as DSFs. The statistical hypothesis testing framework by Fassois and Sakellariou [11] is employed for making decisions about the current structural state. Furthermore, the Mahalanobis distances between DSF vectors from the healthy and the damaged system are directly used for estimation of the approximate damage location. The next section describes the proposed method in detail. Then, numerical simulations of a large WTB under simplified aerodynamic loading with a trailing-edge disbonding damage scenario are presented. The following section shows the results of the SDL. Finally, a discussion of the results and prospects for future work are given.

2. THEORY

The proposed SDD approach assumes that the vibration response signals are stationary. In order to account for loading variability, e.g. due to varying wind speeds in the present case, a normalization of the initial signals can be performed. For a time series, this can be done by removing the estimated mean and dividing by the estimated standard deviation.

The PACF, $\alpha_{zz}[\tau]$, at lag τ describes the correlation between the shifted time series z[t] and z[t-τ] without the effects of intermediate variables z[t-1], z[t-2], …, z[t-τ+1]. For normally distributed time series, the PACF can be given by the correlation in the bivariate conditional probability distribution as [12]:

$$\alpha_{zz}[\tau] = Corr(z[t], z[t-\tau] \mid z[t-1], ..., z[t-\tau+1]) \quad (1)$$

However, the sample PACF, $\hat{\alpha}_{zz}[\tau]$, can be efficiently obtained by the following recursion [12]:

$$\hat{\alpha}_{zz}[\tau] = \frac{\hat{r}_{zz}[\tau] - \sum_{i=1}^{\tau-1} \hat{a}_{\tau-1,i} \hat{r}_{zz}[\tau-i]}{1 - \sum_{i=1}^{\tau-1} \hat{a}_{\tau-1,i} \hat{r}[i]} \quad (2)$$

where $\hat{r}_{zz}[\tau]$ is the sample ACF of the time series z[t] at lag τ, and $\hat{a}_{j,i}$ denotes the estimated j-th AR coefficient of a AR model of order *i*. This shows the close relationship between the PACF, the ACF and AR models. Furthermore, the sample PACF can be directly defined in terms of AR coefficients as:

$$\begin{aligned} \hat{\alpha}_{zz}[1] &= 1 \\ \hat{\alpha}_{zz}[\tau] &= \hat{a}_{\tau,\tau} \end{aligned} \quad (3)$$

In the present study, the SDD phase employs a statistical hypothesis testing approach.

The estimated DSF vectors, $\hat{\mathbf{v}}$, are generally constructed for selected PACF coefficients as

$$\hat{\mathbf{v}} = \left[\hat{\alpha}_{zz}[2] \quad \hat{\alpha}_{zz}[3] \quad \cdots \quad \hat{\alpha}_{zz}[\tau]\right]^T \tag{4}$$

where superscript *T* denotes transpose. The PACF coefficient of lag 1 is omitted because it is always equal to one. It is assumed that the single vector entries are Gaussian distributed. Thus, the difference $\Delta\hat{\mathbf{v}}$ between the estimated DSF vectors of the healthy structure and the current structure, $\hat{\mathbf{v}}_h$ and $\hat{\mathbf{v}}_c$, follows a multivariate Gaussian distribution, $\mathcal{N}(\boldsymbol{\mu}_{\Delta\mathbf{v}}, \boldsymbol{\Sigma}_{\Delta\mathbf{v}})$:

$$\Delta\hat{\mathbf{v}} = \hat{\mathbf{v}}_c - \hat{\mathbf{v}}_h \sim \mathcal{N}(\boldsymbol{\mu}_{\Delta\mathbf{v}}, \boldsymbol{\Sigma}_{\Delta\mathbf{v}}) \tag{5}$$

with the true mean, $\boldsymbol{\mu}_{\Delta\mathbf{v}}$, given as the difference between the true DSF vectors of the healthy and the current structure as

$$\boldsymbol{\mu}_{\Delta\mathbf{v}} = \mathbf{v}_c - \mathbf{v}_h \tag{6}$$

and the true variance-covariance matrix, $\boldsymbol{\Sigma}_{\Delta\mathbf{v}}$, as

$$\boldsymbol{\Sigma}_{\Delta\mathbf{v}} = \boldsymbol{\Sigma}_h + \boldsymbol{\Sigma}_c \tag{7}$$

where $\boldsymbol{\Sigma}_h$ and $\boldsymbol{\Sigma}_c$ are the true variance-covariance matrices of the healthy and current state, respectively.

However, if the current state is also healthy the difference follows a zero-mean multivariate Gaussian distribution with the variance-covariance matrix $\boldsymbol{\Sigma}_{\Delta\mathbf{v}} = 2\boldsymbol{\Sigma}_h$. In this case, the squared Mahalanobis distance, D^2, defined as

$$D^2 = \Delta\hat{\mathbf{v}}^T \boldsymbol{\Sigma}_{\Delta\mathbf{v}}^{-1} \Delta\hat{\mathbf{v}} \sim \mathcal{X}_d^2 \tag{8}$$

follows, as a squared sum of independent Gaussian variables, a central $\mathcal{X}^2$ distribution with *d* degrees-of-freedoms (DOFs), $\mathcal{X}_d^2$. The number of DOFs is equal to the number of the selected PACF coefficients included in the DSF vector. The true variance-covariance matrix is generally unavailable, thus the estimated version, $\hat{\boldsymbol{\Sigma}}_{\Delta\mathbf{v}}$, is used instead.

The hypothesis testing problem can be defined as

$$\begin{aligned} H_0: &\quad \Delta\mathbf{v} = \mathbf{v}_c - \mathbf{v}_h = \mathbf{0} \quad (\textit{healthy}) \\ H_1: &\quad \Delta\mathbf{v} = \mathbf{v}_c - \mathbf{v}_h \neq \mathbf{0} \quad (\textit{damaged}) \end{aligned} \tag{9}$$

where the null hypothesis, H_0, describes the healthy state and the alternative hypothesis, H_1, the damaged state. This enables to define a statistical test on the squared Mahalanobis distance by means of the cumulative $\mathcal{X}^2$ distribution function, $F_{\mathcal{X}_d^2}$, as

$$\begin{aligned} D^2 < F_{\mathcal{X}_d^2}(1-\alpha) &\Rightarrow H_0 \text{ is accepted} \\ \text{Else} &\Rightarrow H_0 \text{ is rejected} \end{aligned} \tag{10}$$

where α is the selected level of significance.

However, SDD is the basic level of diagnostics which only enables to detect if damage occurred or not. A SHM technique should ideally provide additional information in order to maximise its benefits with respect to safety and economics. The estimation of the damage location is the second level of diagnostics. It can be hypothesised that the signals from sensors closest to the damage are more affected by the damage than others and the PACF-based DSF can be used for SDL. Statistical hypothesis testing, as proposed for SDD, may not be useful because signals from sensor further apart will also experience noticeable changes due to damage especially for more significant alterations. Therefore, the direct use of the squared Mahalanobis distance, as defined by Eq. 13, is proposed for SDL. Comparison of distances obtained from different sensor locations enables to identify the location of the most significant change, and with it, the damage location.

3. SIMULATIONS

The Sandia National Laboratory (SNL), USA designed a 61.5 m reference WTB [13] according to the specifications of the 5 MW reference WT [14] of the National Renewable Energy Laboratory (NREL), USA. With the help of the SNL software package NuMAD [15], an ANSYS Mechanical [16] FE model of this large WTB was created for the present study. The FE model with 1,650 SHELL281 elements was judged as adequate with respect to the approximation of vibration responses. A parked WT situation is assumed for the simulation of the single WTB and tower motions are also ignored.

Due to the production process of WTBs, where upper and lower shells are bonded together, disbonding in the trailing-edge bondline is critical. This is especially the case for large WTBs [2], because they are disposed to trailing-edge buckling [17]. Furthermore, failures in trailing-edge bonding were also investigated by inspections of 100 kW and 300 kW WTs in Egypt [18], where the maximum chord location was found to be damage prone. Therefore, this location is chosen as the damage initiation point with extension towards the WTB's tip, as shown in Figure 1. A separation of nodes between FEs at

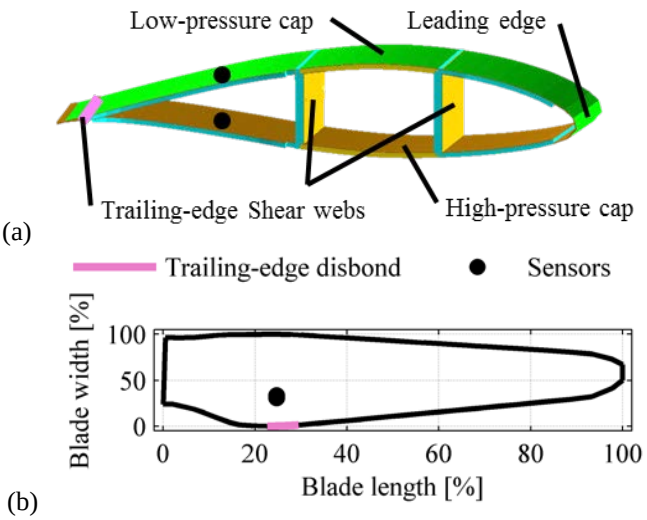

Figure 1: Damage and sensor location in WTB: (a) cross section, (b) top view

the selected locations is used to introduce a damage scenario into the FE model. The number of separated nodes corresponds to the damage extent, and with it, to the length of the disbond.

The proposed SDD method is based on time series analysis, thus transient dynamic simulations are performed to generate response acceleration time series. The use of realistically simulated excitations is paramount for investigating the performance and applicability of vibration-based SHM techniques. Therefore, a three-step simplified aerodynamic loading approach was developed.

First, full-field wind data are generated with the NREL software TurbSim [19] according to IEC 61400-1 3rd Ed. [20]. The mean wind speed of 10 m/s at the hub height is selected as the average wind speed of an IEC Type I WT. For the wind category B and the normal turbulence model, the resulting turbulence intensity of the inflow wind component is 18.34%.

The second step is the calculation of aerodynamic loads with the NREL software packages AeroDyn [21] and FAST [22]. The blade element momentum theory is selected for modelling the wake effect. Seventeen strip elements with constant aerodynamic and structural properties are used to approximate the WTB for these simulations. The result are time series of lift and drag forces, F_N and F_T, respectively, and pitching moments, M_P, at the element centres (x_r,y_r,z_r) as illustrated in Figure 2.

The application of these element loads in a FE model requires a mapping to nodal forces, $f_{x,i}$ and $f_{y,i}$, of the WTB's surface nodes, which is done in the third step. This mapping is based on Berg et al. [23]. A system of linear equations can be established for the equilibrium equations of forces and moments for each WTB element. Non-zero pitching moments in y-direction and linear spatial distribution are chosen because the mapping is generally not unique. Solving the linear system of equations numerically enables to calculate load coefficients for the nodal forces for each surface node in advance. Then, only simple evaluations are required for every load step during the transient dynamic simulations, where a constant time step of 0.005 s is chosen.

4. RESULTS

Initially, numerical modal analysis of the healthy WTB is performed in order to investigate the dynamic behaviour of the structure. The high flexibility of the WTB is indicated by the low natural frequencies as given in Table 1, where the mode shapes are also shown.

Then, the effect of trailing-edge disbonding on modal properties is assessed for the damaged WTB FE models with respect to the healthy state system. The extent of the disbonding is varied in eleven steps with length of approx. 0.4 m, where the maximum extent becomes 4.5 m or 7.4% of the length of the WTB. The relative difference, Δf_i, between the natural frequencies of

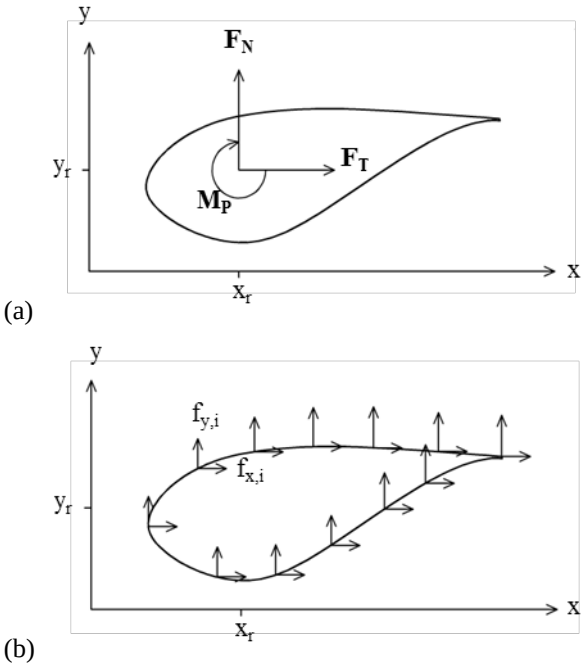

Figure 2: Aerodynamic loads on blade cross section: (a) element forces, and (b) nodal forces

Table 1: Numerical modal analysis results of the healthy WTB for the first three modes

Mode Description	Natural Frequency	Mode Shape Views
1st mode in flap-wise bending	0.87 Hz	Edge-wise  Flap-wise 
1st mode in edge-wise bending	1.06 Hz	Edge-wise  Flap-wise 
2nd mode in flap-wise bending	2.67 Hz	Edge-wise  Flap-wise 

the healthy, $f_{h,i}$, and the damaged model, $f_{d,i}$, gives the effect of damage on the i-th frequency as

$$\Delta f_i = (f_{h,i} - f_{d,i}) / f_{h,i} \times 100\% \qquad (11)$$

Figure 3a shows these effects for the first ten natural frequencies, where contributions of the first four frequencies are invisible due to their minor changes. Further, it can be seen that the cumulative sum of relative frequency differences and the disbond length have a monotonic nonlinear relationship. For the selected disbonding damage scenario, modes with frequencies of the healthy system higher than 8 Hz have the highest contribution to the cumulative sum of relative differences.

Additionally, the wind speed amplitude spectrum of the inflow wind component at the hub position is given as reference for the aerodynamic excitation in Figure 3b. The realization of the inflow wind component is simulated with TurbSim for 630 s based on the Kaimal spectrum and a mean wind speed of 10 m/s. The Kaimal spectrum adopted has a low frequency excitation characteristic, which is important with respect to the changes in the natural frequencies due to damage. It can be noticed that the significant changes of the higher modes will have only a minor contribution to the damage detectability as these modes will be weakly excited and would not be clearly identified from output-only data. Only modes with frequencies less than 8 Hz can be assumed to be sufficiently excited to affect the damage detectability. This means for a disbond of 7.4% of the WTB length the cumulative relative frequency difference is less than 2%, which illustrates the challenge of vibration-based SDD for this structure.

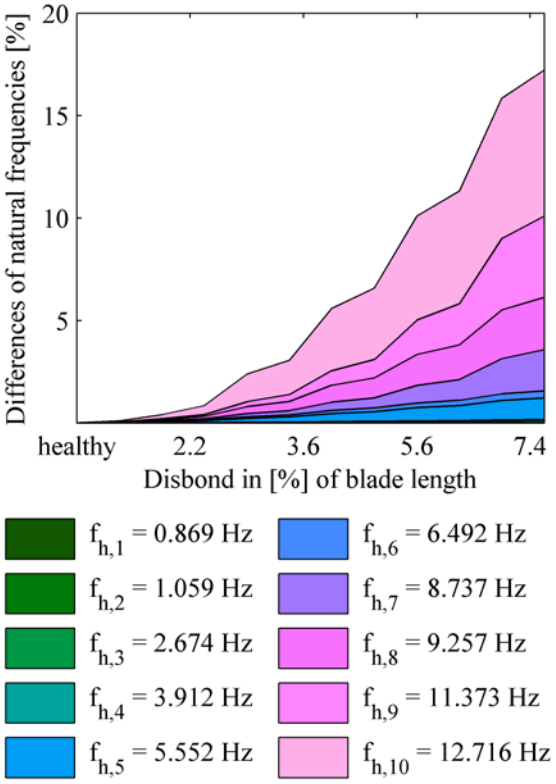

(a)

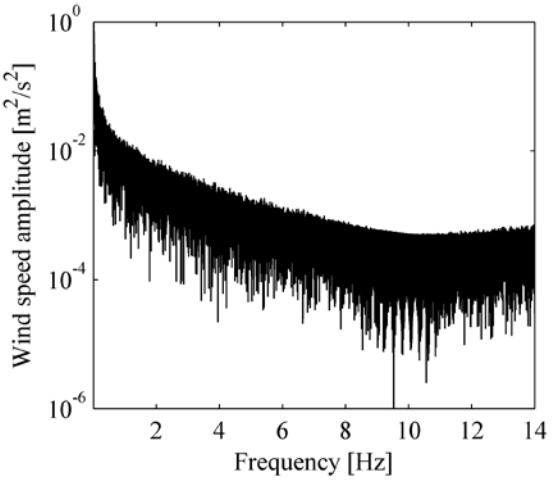

(b)

Figure 3: (a) Cumulative relative differences of natural frequencies with increasing trailing-edge disbanding, and (b) Wind speed amplitude spectrum for simulated inflow wind component

For the following discussion of time series modelling with PACFs and SDL, transient dynamic simulations are performed for the healthy and damaged WTB FE models. Flap-wise and edge-wise accelerations at selected nodes are obtained for a durations of 630 s. Flap-wise signals for the two nodes indicated as 'Sensors' in Figure 1 are primarily used in the following. These sensors are located approx. 1.5 m from the selected disbonding damage scenario. Each time series is divided into 100 segments of 6,000 samples with a shift of 1,200 samples. The time series segments are directly used without additional filtering or subsampling. Nevertheless, each unprocessed segment is normalised by its estimated mean and standard deviation in order to account for variations of the aerodynamic excitation.

The estimates of the PACF for acceleration responses from the sensors at the low-pressure and high-pressure caps are shown in Figure 4. The results are given in terms of the mean and standard deviation obtained from the time series segments of the healthy system. It can be seen that the coefficient mean values decrease with increasing number of lags while the standard deviations increase. For the following analysis, the DSF vector is therefore defined by the PACF coefficients from two to 40 in order to limit the effect of variations from the single coefficients.

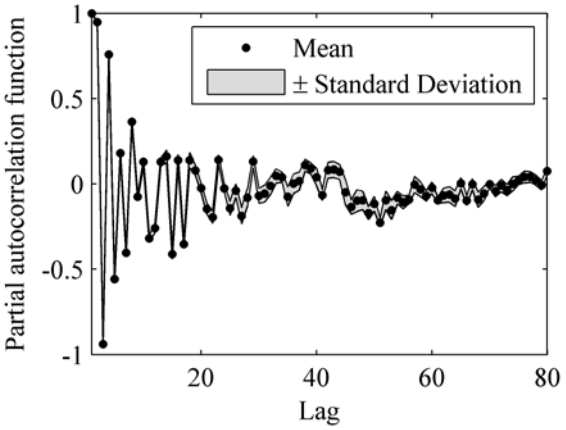

(a)

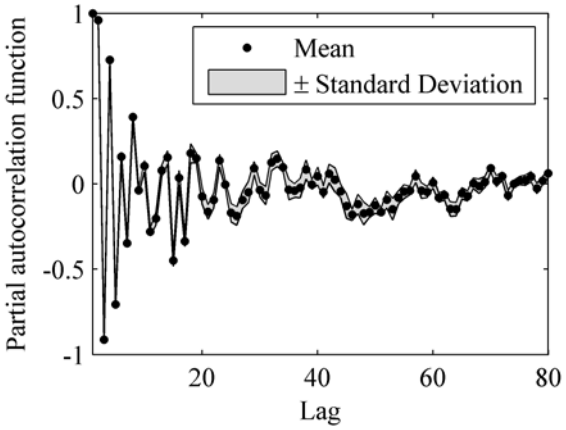

(b)

Figure 4: Mean and standard deviation of PACF from flap-wise acceleration time series segments of the healthy WTB: (a) low-pressure cap sensor, and (b) high-pressure cap sensor

This definition of the DSF vector enables to perform SDD for the WTB with increasing trailing-edge disbonding. The statistical threshold is defined by the value of $F_{\chi^2_{39}}(95\%)$. The results are given in Table 2 in terms of the relative rejection rates of the null hypothesis, where a value of 0% indicates that no damage is detected from the time series segments. Correspondingly, damage is detected in each time series segment if the relative rejection rate is 100%. With this definition, it can be seen that both sensors enable to detect damages as small as 1.4% disbonding of the blade length. However, the location at the low-pressure cap is a bit more sensitive to damage because the relative rejection rate for a disbond of 0.7% blade length is higher than the result obtained from the high-pressure cap sensor.

The previous results were obtained from non-noisy signals. However, real records of acceleration signals are normally polluted with noise coming from the acceleration sensors and the data acquisition electronics. Therefore, a further analysis was performed, where noise is artificially added to the time series segments. The artificial noise is introduced to the simulated signals as Gaussian random sequences with a

Table 2: Relative rejection rates of H_0 without noise

Damage extent in [%] of blade length		Low-pressure cap sensor	High-pressure cap sensor
0.0	H_0	0.0	0.0
0.7	H_1	30.0	2.0
1.4	H_1	100.0	100.0
2.2	H_1	100.0	100.0
2.9	H_1	100.0	100.0
3.6	H_1	100.0	100.0
4.3	H_1	100.0	100.0
5.0	H_1	100.0	100.0
5.6	H_1	100.0	100.0
6.2	H_1	100.0	100.0
6.8	H_1	100.0	100.0
7.4	H_1	100.0	100.0

standard deviation equal to the standard deviation of the initial signal multiplied by a noise-to-signal ratio of 2%. Table 3 gives the results for the selected sensors. It can be seen that the artificial noise adversely affects the detectability of early damages, where a disbond with 2.2% blade length is reliably detected by both sensors compared to 1.4% in the unpolluted case. Furthermore, the low-pressure cap sensor shows again a slightly better performance than the high-pressure cap sensor.

Table 3: Relative rejection rates of H_0 with 2% noise

Damage extent in [%] of blade length		Low-pressure cap sensor	High-pressure cap sensor
0.0	H_0	0.0	0.0
0.7	H_1	0.0	4.0
1.4	H_1	49.0	39.0
2.2	H_1	100.0	96.0
2.9	H_1	100.0	100.0
3.6	H_1	100.0	100.0
4.3	H_1	100.0	100.0
5.0	H_1	100.0	100.0
5.6	H_1	100.0	100.0
6.2	H_1	100.0	100.0
6.8	H_1	100.0	100.0
7.4	H_1	100.0	100.0

SDD is only the first level of structural health diagnostics and enables to identify the presence of damages. However, for practical applications, the identification of the damage location is paramount. Thus, the performance of the proposed DSF is assessed with respect to SDL. It is proposed to use directly the Mahalanobis distances for SDL. Nevertheless, for comparison of results from simulations with different extents of disbond, two additional processing steps were performed. First, the mean values of the distances estimated from time series segments of each sensor location for simulations of the same damage extent were calculated.

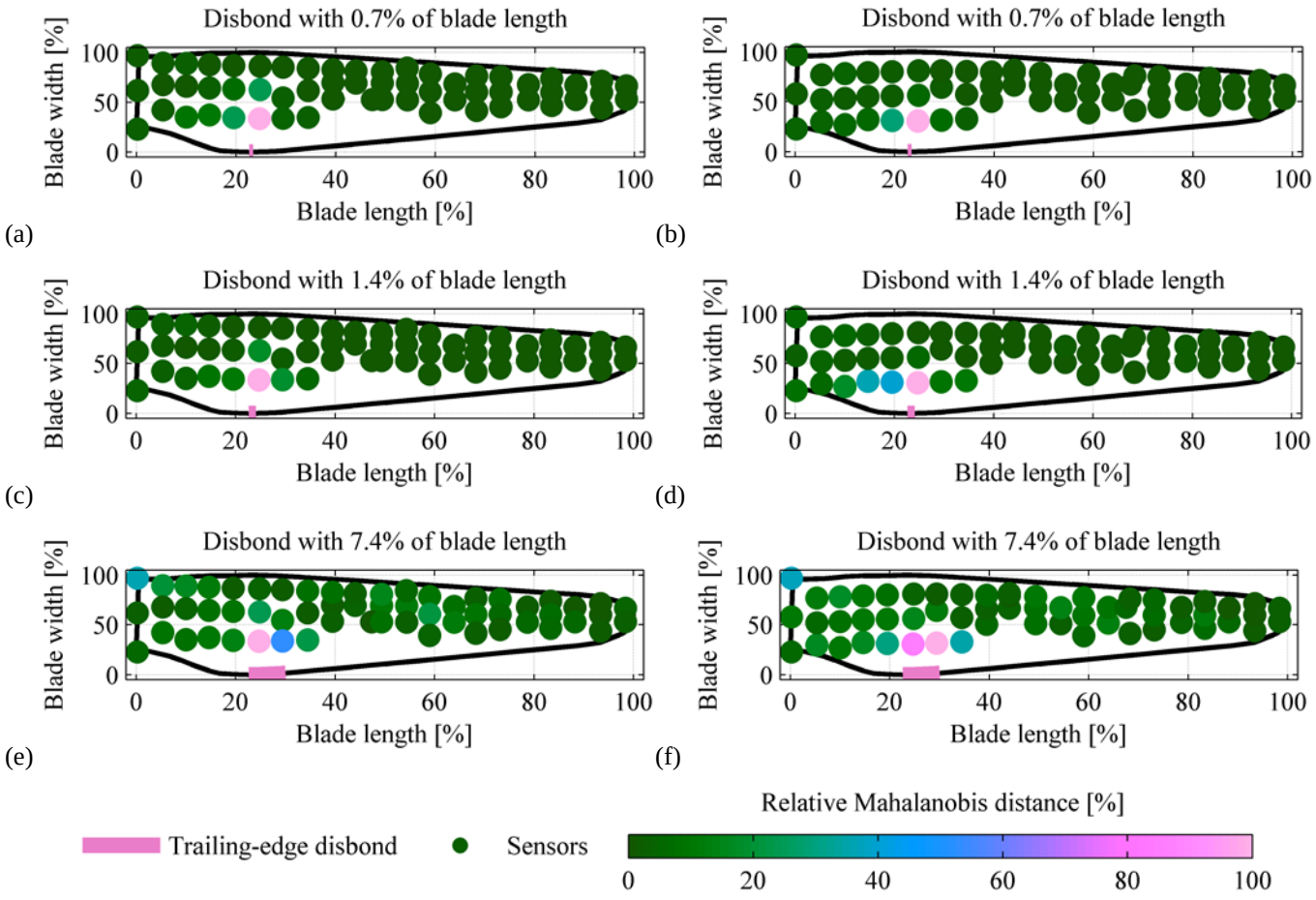

Figure 5: Relative Mahalanobis distances for PACF-based DSF of flap-wise acceleration responses: (a, c, e) low-pressure cap sensors, and (b, d, f) high-pressure cap sensors

Second, the relative Mahalanobis distances were obtained by scaling the estimated mean values to the range between 0% and 100%. This was done for selected sensors from the high-pressure and low-pressure caps separately. The results are given in Figure 5, where the positions of the points represent the sensor locations, and the colours illustrate the relative distances.

It can be seen that the highest relative distances are present at sensor locations closest to the damage, which supports the initial assumption that signals from these sensors are more affected by damage. This is even for the case for the scenario with a disbonding extent of only 0.7% of the blade length, where statistical hypothesis testing did not enable to detect damage. Furthermore, comparing the results for a disbond with 1.4% and 7.4% blade length illustrates that the proposed method allows tracking the growth of the disbond. This behaviour is more significant for the high-pressure cap sensors. Nevertheless, the results from both caps are comparable.

5. CONCLUSIONS

The present study demonstrated the application of a PACF-based DSF and statistical hypothesis testing for SDD in a large WTB. Decisions about the structural state were obtained via statistical hypothesis testing using the Mahalanobis distances between vectors of PACF coefficients estimated from acceleration response signals. Furthermore, Mahalanobis distances for signals from sensors of different locations were used for estimation of the approximate damage locations. A FE model of large WTB was used to perform transient dynamic simulations. In order to apply a realistic excitation without excessive computational efforts, a simplified aerodynamic loading approach was utilized. The initial healthy WTB was modified with a realistic trailing-edge disbonding damage scenario with several extents.

The effect of trailing-edge disbonding was initially investigated by modal analysis. It was shown that the most significant changes are related to modes of higher frequencies. These modes are less excited by the low frequencies characteristics of aerodynamic loading and their natural frequencies would not be suitable as DSFs.

SDD was performed, where a statistical model represented by a certain mean vector and variance-covariance matrix was estimated from the PACF-based DSF vector. Then, statistical hypothesis testing using the Mahalanobis distances between the healthy and damages features was used for making decisions about the current structural state. The detectability of damage for increasing disbond extent was assessed by relative rejection rates of the null hypothesis. The proposed DSF enabled to detect disbonds of approx. 1.4% and 2.2% for signals with and without artificial noise, respectively.

A further aspect of the present paper is SDL based on the direct use of Mahalanobis distances estimated from different sensor locations along the WTB. This follows the assumption that signals of sensors close to the damage are more affected by the damage than others. Due to the significant change in that distance for sensor close to the damage compared to others, it was shown that the approximate damage location could be estimated even in the case where no statistical evidence of damage was determined. It was also found that for increasing disbond lengths more sensors were significantly affected giving additional information about damage charter.

This paper illustrated the performance of a novel PACF-based DSF with respect to SDD and SDL in large WTB. It was demonstrated that this DSF in a statistical hypothesis testing framework enabled to detect a disbonding damage of small size. Furthermore, the performance for SDL was shown, where it was possible to estimate the approximate damage location. These findings are promising for future developments of SDD/SDL methods as part of SHM systems in WTBs. However, further research is required to increase the detectability of early damages and accuracy of damage location estimates using additional numerical simulations and experimental studies.

ACKNOWLEDGEMENT

Piotr Omenzetter and Simon Hoell's work within the Lloyd's Register Foundation Centre for Safety and Reliability Engineering at the University of Aberdeen is supported by Lloyd's Register Foundation. The Foundation helps to protect life and property by supporting engineering-related education, public engagement and the application of research.

REFERENCES

1. THE EUROPEAN PARLIAMENT AND THE COUNCIL OF THE EUROPEAN UNION, 2009 'The Renewable Energy Directive 2009/28/EC', *Official Journal of the European Union, L 140.*

2. JENSEN FM, SØRENSEN JD, NIELSEN PH, BERRING P, FLORESE S, 2011 'Failures in Trailing Edge Bondlines of Wind Turbine Blades', *The 32nd Risø International Symposium on Materials Science, 32, 319-27*.

3. BLANCO MI, 2009 'The Economics of Wind Energy', *Renewable and Sustainable Energy Reviews, 13, 1372-82*.

4. CHOU JS, CHIU CK, HUANG IK, CHI KN, 2013 'Failure Analysis of Wind Turbine Blade Under Critical Wind Loads', *Engineering Failure Analysis, 27, 99-118.*

5. SCHUBEL PJ, CROSSLEY RJ, BOATENG EKG, HUTCHINSON JR, 2013 'Review of Structural Health and Cure Monitoring Techniques for Large Wind Turbine Blades', *Renewable Energy, 51, 113-23.*

6. CARDEN EP, FANNING P, 2004 'Vibration Based Condition Monitoring: A Review', *Structural Health Monitoring, 3, 355-77.*

7. REYNDERS E, 2012 'System Identification Methods for (Operational) Modal Analysis: Review and Comparison', *Archives of Computational Methods in Engineering, 19, 51-124.*

8. NAIR KK, KIREMIDJIAN AS, LAW KH, 2006 'Time Series-Based Damage Detection and Localization Algorithm with Application to the ASCE Benchmark Structure', *Journal of Sound and Vibration, 291, 349-68.*

9. HÄCKELL MW, ROLFES R, 2013 'Monitoring a 5 MW Offshore Wind Energy Converter - Condition Parameters and Triangulation Based Extraction of Modal Parameters', *Mechanical Systems and Signal Processing, 40, 322-43.*

10. HOELL S, OMENZETTER P, 2014 'Damage Detection in a Wind Turbine Blade Based on Time Series Methods', *7th European Workshop on Structural Health Monitoring (EWSHM), 1-8.*

11. FASSOIS SD, SAKELLARIOU JS, 2007 'Time-series Methods for Fault Detection and Identification in Vibrating Structures', Philosophical Transactions of the Royal Society A: Mathematical, Physical and Engineering Sciences 2007; 365:411-48.

12. CRYER JD, CHAN K, 2008 'Time Series Analysis with Applications in R', *New York, NY, USA, Springer Science+Business Media, LLC.*

13. RESOR BR, 2013 'Definition of a 5MW/61.5m Wind Turbine Blade Reference Model', *Albuquerque, New Mexico, USA, Sandia National Laboratories, SAND2013-2569 2013.*

14. JONKMAN JM, BUTTERFIELD S, MUSIAL W, SCOTT G, 2009 'Definition of a 5-MW Reference Wind Turbine for Offshore System Development', *Golden, Colorado, USA, National Renewable Energy Laboratory, NREL/TP-500-38060 2009*.

15. BERG JC, RESOR BR, 2012 'Numerical Manufacturing and Design Tool (NuMAD v2.0) for Wind Turbine Blades: User's Guide', *Albuquerque, New Mexico, USA, Sandia National Laboratories, SAND2012-7028 2012*.

16. SAS IP INC, 2012 'ANSYS Mechanical APDL Theory Reference'.

17. JENSEN FM, KLING A, SØRENSEN JD, 2012 'Scale-Up of Wind Turbine Blades - Changes in Failure Type', *Proceedings of EWEA Annual Event (EWEA 2012), 1-6.*

18. ATAYA S, AHMED MMZ, 2013 'Damages of Wind Turbine Blade Trailing Edge: Forms, Location, and Root Causes', *Engineering Failure Analysis, 35, 480-8.*

19. KELLEY N, JONKMAN B, 2013 'TurbSim', *National Wind Technology Center, USA, v1.06.00, Last modified 30-May-2013, accessed 14-October-2013.*

20. IEC TECHNICAL COMMITTEE 88: WIND TURBINES, 2005 'International Standard IEC 61400-1.

21. LAINO DJ, 2013 'AeroDyn', *National Renewable Energy Laboratory, USA, v13.00.02a-bjj, Last modified 23-February-2013, accessed 15-October-2013.*

22. JONKMAN J, 2013 'FAST', *National Wind Technology Center, USA, v7.02.00d-bjj, Last modified 28-October-2013, accessed 28-October-2013.*

23. BERG JC, PAQUETTE JA, RESOR BR, 2011 'Mapping of 1D Beam Loads to the 3D Wind Blade for Buckling Analysis', *Collection of Technical Papers - AIAA/ASME/ASCE/AHS/ASC Structures, Structural Dynamics and Materials Conference 2011, 1-8.*